Generation and Reactivity of Unsaturated Iridium and Rhodium Dimethyl Complexes

Eric G. Lundquist, Kirsten Folting, John C. Huffman, and Kenneth G. Caulton*

Department of Chemistry and Molecular Structure Center, Indiana University, Bloomington, Indiana 47405

Received December 19, 1989

Protonation ($HBF_4 \cdot OEt_2$) of MMe_3P_3 (M = Rh, Ir; P = PMe_2Ph) in CH_2Cl_2 gives CH_4 and *cis,mer*-$MMe_2P_3BF_4$, characterized as a fluxional (methyl site exchange) molecular η^1-BF_4 species by ^1H, ^{31}P, ^{19}F, and ^{11}B NMR studies and (for M = Ir) X-ray diffraction. Crystal data for $IrMe_2P_3BF_4 \cdot C_6H_6$ (-100 °C): a = 16.708 (6) Å, b = 9.332 (2) Å, c = 23.214 (8) Å, β = 110.05 (2)°, with Z = 4 in space group $P2_1/c$. Ethylene replaces BF_4^- to give (at 25 °C) $[IrMe_2(C_2H_4)P_3]BF_4$ and (at 50 °C) $[Ir(C_2H_4)_2P_3]BF_4$ and C_2H_6. Carbon monoxide replaces BF_4 to give first $[IrMe_2(CO)P_3]BF_4$ and then $IrMe[C(O)Me](CO)P_3^+$. Ethylene reacts (25 °C) with $RhMe_2P_3BF_4$ to immediately give ethane and $[RhP_4]BF_4$. Carbon monoxide replaces BF_4^- to give first $RhMe_2(CO)P_3^+$ and then acetone and $[RhP_4]BF_4$. Ethylene also promotes acetone elimination from $RhMe_2(CO)P_3^+$, to again generate RhP_4^+. All of the above are characterized by multinuclear NMR and vibrational spectroscopy and, for $[IrMe_2(C_2H_4)P_3BF_4$, X-ray diffraction. Crystal data (-155 °C): a = 13.373 (4) Å, b = 12.242 (3) Å, c = 18.139 (b) Å, with Z = 4 in space group $P2_1cn$.

Introduction

The creation of an open coordination site in a transition-metal complex has been a longstanding objective. This may be achieved by thermal or photoinduced dissociation of a Lewis base or by reductive elimination or by electrophilic (e.g., H^+, R^+, Ag^+, Tl^+) abstraction of what is formally an anionic species (e.g., halide, H^-, or R^-). The electrophilic abstraction, since it requires a counterion, raises the question of the identity of the ideal noncoordinating anion;[1] only when this problem is solved will the generation of authentic unsaturation be realized. A related factor is the search for the ideal solvent, being one that will dissolve the ionic reactants and products yet will not coordinate to the transition-metal orbital liberated in the electrophilic abstraction. Acetonitrile has proven itself unsuitable in this regard,[2-4] while CH_2Cl_2 may have its successes.[5,6] There are, however, claims of coordination of CH_2Cl_2,[7-9] and halocarbons have been demonstrated to coordinate through halogen lone pairs.[10-13] Related complications arose when $[Ph_3C]BF_4$ was employed in an attempt to abstract H^- from CpRe(NO)(CO)H: triphenylmethane occupies a coordination site on rhenium.[14]

These problems notwithstanding, electrophilic abstraction has been productive of much substitution chemistry in the organometallic field. The work of the group of Beck has been outstanding in this regard, with their focus being the species $M(CO)_5X$ (M = Mn, Re) and $CpM'L_3X$ (M' = Mo, W), where X = H, Me.[15,16] Both Beck[16] and Cutler[13] have used the resulting "incipient Lewis acids" to attack metal acyl complexes, yielding unusual μ-acyl species. Recently, Jordan[17] and others[18] have used such electrophilic abstraction to generate reactive early-transition-metal alkyl cations capable of olefin polymerization. With the exception of such reports, however, there has been little work creating unsaturation in the presence of reactive (e.g., migration-prone) coligands such as H or CH_3. We have previously been successful generating reactive unsaturated hydride species via protonation of polyhydride complexes[6,19,20] and now turn our attention toward the production of unsaturated alkyl complexes by protonation of polyalkyl compounds. This approach allows us ready access to the area of unsaturated alkyl complexes relevant to olefin polymerization or hydroformylation. We report here on the structure and comparative reactivity of the complexes $MMe_2P_3BF_4$ (M = Rh, Ir; P ≡ PMe_2Ph) formed by stoichiometric protonation of *fac*-MMe_3P_3.

Experimental Section

All manipulations were carried out with use of standard Schlenk and glovebox procedures under prepurified nitrogen or vacuum. Solvents (THF, benzene, toluene, pentane) were dried and deoxygenated by Na/K benzophenone and vacuum transferred prior to use. CD_2Cl_2 and CH_2Cl_2 were distilled from P_2O_5. MeMgCl, MeLi, and $HBF_4 \cdot OEt_2$ were purchased from Aldrich. The gases C_2H_4 (CP grade, Matheson), $^{13}C_2H_4$ (99% ^{13}C, Cambridge Isotope Laboratories), CO (Ultra High Purity, Air Products), and ^{13}CO (99% ^{13}C, Mound Research) were used as received. ^1H, ^{31}P, and ^{13}C NMR spectra were recorded on a Nicolet NT-360 spectrometer at 360, 146, and 100 MHz, respectively. ^{11}B and ^{19}F NMR spectra were also recorded on a Nicolet NT-360 spectrometer at 116 and 339 MHz. Two-dimensional NMR experiments were performed on a Bruker AM-500 spectrometer. Infrared spectra were recorded on a Perkin-Elmer 283 spectrophotometer. Where noted, precise

(1) Shelly, K.; Reed, C. A.; Lee, Y. J.; Scheidt, W. R. *J. Am. Chem. Soc.* **1986**, *107*, 3117.
(2) Rhodes, L. F.; Zubkowski, J. D.; Folting, K.; Huffman, J. C.; Caulton, K. G. *Inorg. Chem.* **1982**, *21*, 4185.
(3) Bruno, J. W.; Huffman, J. C.; Caulton, K. G. *J. Am. Chem. Soc.* **1984**, *106*, 1663.
(4) Rhodes, L. F.; Green, M. A.; Huffman, J. C.; Caulton, K. G. In *Chemistry and Uses of Molybdenum*; Barry, H. F., Mitchell, P. C. H., Climax-Molybdenum Co.: Ann Arbor, MI, 1982; p 79.
(5) Rhodes, L. F.; Caulton, K. G. *J. Am. Chem. Soc.* **1985**, *107*, 259.
(6) Lundquist, E. G.; Huffman, J. C.; Folting, K.; Caulton, K. G. *Angew. Chem., Int. Ed. Engl.* **1988**, *27*, 1165.
(7) Beck, W.; Schloter, K. *Z. Naturforsch.* **1978**, *33B*, 1214.
(8) Winter, C. H.; Arif, A. M.; Gladysz, J. A. *J. Am. Chem. Soc.* **1987**, *109*, 7560.
(9) Mattson, B. M.; Graham, W. A. G. *Inorg. Chem.* **1981**, *20*, 3186.
(10) Burk, M. J.; Segmuller, B.; Crabtree, R. *Organometallics* **1987**, *6*, 2241 and references therein.
(11) Czech, P. T.; Gladysz, J. A.; Fenske, R. F. *Organometallics* **1989**, *8*, 1806 and references therein.
(12) Winter, C. H.; Veal, W. R.; Garner, C. M.; Arif, A. M.; Gladysz, J. A. *J. Am. Chem. Soc.* **1989**, *111*, 4766.
(13) Cutler, A. R.; Todaro, A. B. *Organometallics* **1988**, *7*, 1782.
(14) Sweet, J. R.; Graham, W. A. G. *Organometallics* **1983**, *2*, 135.
(15) Sünkel, K.; Urban, G.; Beck, W. *J. Organomet. Chem.* **1983**, *252*, 187.
(16) Beck, W.; Sünkel, K. *Chem. Rev.* **1988**, *88*, 1405.
(17) Jordan, R. F.; LaPointe, R. E.; Bajgur, C. S.; Echols, S. F.; Willett, R. *J. Am. Chem. Soc.* **1987**, *109*, 4111.
(18) (a) Lin, Z.; LeMarechal, J. F.; Sabat, M.; Marks, T. J. *J. Am. Chem. Soc.* **1987**, *109*, 4127. (b) A reviewer has commented "...if xenon is a ligand for iridium, it is going to be hard to achieve a true 16-valence electron count by any means". See: Weiller, B. H.; Wasserman, E. P.; Bergman, R. G.; Moore, C. B.; Pimentel, G. C. *J. Am. Chem. Soc.* **1989**, *111*, 8288.
(19) Johnson, T. J.; Huffman, J. C.; Caulton, K. G.; Jackson, S. A.; Eisenstein, O. *Organometallics* **1989**, *8*, 2073.
(20) Marinelli, G.; Rachidi, I.; Streib, W. E.; Eisenstein, O.; Caulton, K. G. *J. Am. Chem. Soc.* **1989**, *111*, 2396.

0276-7333/90/2309-2254$02.50/0

Table I. Crystal Data for $IrMe_2(PMe_2Ph)_3BF_4 \cdot C_6H_6$ and $[IrMe_2(C_2H_4)(PMe_2Ph)_3]BF_4$

empirical formula	$C_{32}H_{45}BF_4P_3Ir$	$C_{28}H_{43}BF_4P_3Ir$
color	pale yellow	colorless
cryst dimens, mm	0.07 × 0.07 × 0.15	0.25 × 0.25 × 0.25
space group	$P2_1/c$	$P2_1cn$
cell dimens		
temp, °C	−100	−155
a, Å	16.708 (6)	13.373 (4)
b, Å	9.332 (2)	12.242 (3)
c, Å	23.214 (8)	18.139 (6)
β, deg	110.05 (2)	
molecules/cell	4	4
volume, Å^3	3400.06	2969.73
calcd density, g/cm^3	1.564	1.681
wavelength, Å	0.710 69	0.710 69
mol wt	801.65	751.99
linear abs coeff, cm^{-1}	40.885	46.806
max abs	0.743	
min abs	0.627	
no. of unique intens	4442	2058
no. with $F > 0.0$	4181	1855
no. with $F > 2.33(F)$	3898	1580
R for averaging	0.094	0.049
final residuals		
$R(F)$	0.0622	0.0540
$R_w(F)$	0.0622	0.0498
goodness of fit for the last cycle	1.67	1.00
max Δ/σ for last cycle	0.55	0.55

quantities of gases were determined with use of a standard calibrated gas manifold. The products reported here have been identified and characterized by X-ray diffraction and by ^1H, ^{31}P, and ^{13}C NMR spectra. Since the solid samples dissolved *completely* in the NMR solvents employed, and since they are interrelated by a cycle of chemical transformations, we do not offer supplemental proof of composition by elemental analysis.

Protonation of *fac*-$IrMe_3P_3$. Generation of $IrMe_2P_3BF_4$. A 5-mm NMR tube was charged with $IrMe_3P_3$[21-23] (75 mg, 0.12mmol) and CD_2Cl_2 (0.5 mL), and against a N_2 flow, 1 equiv of $HBF_4 \cdot OEt_2$ (12 μL, 0.12 mmol) was added. This caused immediate gas evolution and the formation of a yellow solution. This solution was thermochromic, becoming colorless below −20 °C. ^1H NMR spectroscopy indicated quantitative conversion to $IrMe_2P_3BF_4$. ^1H NMR (360 MHz, 25 °C, CD_2Cl_2): δ 0.50 (br q, J_{Me-P} = 4 Hz, $Ir(Me)_2$, 6 H), 1.6 (br s, P–Me, 18 H), 7.2–7.5 (br m, P–Ph). $^{31}P\{^1H\}$ (146 MHz, 19 °C, CD_2Cl_2): δ −29.0 (br s, 2 P), −44.0 (br s, 1 P). Low-temperature ^1H NMR (360 MHz, −80 °C, CD_2Cl): δ 0.40 (br m, Ir–Me, 3 H), 0.60 (br m, Ir–Me, 3 H), 1.25 (m, Me–P, 6 H), 1.7 (m, Me–P, 6 H), 1.8 (m, Me–P, 6 H), 7.2–7.6 (m, P–Ph). Low-temperature $^{31}P\{^1H\}$ (146 MHz, −80 °C, CD_2Cl): δ −29.0 (d, J_{PP} = 15 Hz, 2 P), −44.0 (t, J_{PP} = 15 Hz, 1 P). ^{11}B NMR (116 MHz, 24 °C, CD_2Cl_2) δ −1.37 (br s). (24 °C, toluene): δ −0.27 (br s). ^{19}F NMR (339 MHz, 24 °C, CD_2Cl_2): δ −153 (sharp s). ^{19}F NMR (24 °C, toluene): δ −170 (s). Low-temperature ^{19}F NMR (339 MHz, −90 °C, CD_2Cl_2): δ −153 (sharp s). Low-temperature ^{19}F NMR (−90 °C, toluene): −185 (br s, half-width 6800 Hz).

Crystallography of $IrMe_2(PMe_2Ph)_3BF_4 \cdot C_6H_6$. A suitable crystal, grown by layering a 0.3 M benzene solution with pentane, was transferred to the goniostat with use of standard inert-atmosphere handling techniques and cooled to −100 °C for characterization and data collection.[24] When it was cooled, the crystal changed from pale yellow to nearly colorless. At approximately −120 °C, the crystals underwent a (destructive) phase transition. A systematic search of a limited hemisphere of reciprocal space located a set of diffraction maxima with symmetry and systematic absences corresponding to the unique monoclinic space group $P2_1/c$. Subsequent solution and refinement of the structure confirmed this choice. Data were collected ($6° \le 2\theta \le 45°$) with use of a continuous θ–2θ scan with fixed backgrounds and were reduced to a unique set of intensities and associated σ values in the usual manner.[24] An absorption correction was performed. Parameters of the crystal and the data are shown in Table I.

The structure was solved by a combination of direct methods (MULTAN78) and Fourier techniques and revealed a benzene molecule in the crystal lattice. A difference Fourier synthesis revealed the location of some, but not all, hydrogen atoms. All hydrogen atom positions were therefore calculated with use of

Table II. Fractional Coordinates and Isotropic Thermal Parameters[a] for $IrMe_2(PMe_2Ph)_3BF_4$

	10^4x	10^4y	10^4z	$10B_{iso}$, Å^2
Ir1	3024.6 (3)	3055 (1)	4598.6 (2)	17
C2	4247 (8)	2404 (16)	4581 (7)	34
C3	3638 (8)	4826 (16)	5106 (6)	30
F4	2275 (5)	1142 (8)	3956 (4)	33
B5	2125 (11)	−218 (17)	3648 (8)	30
F6	1942 (6)	10 (10)	3042 (4)	46
F7	1443 (6)	−833 (10)	3762 (4)	47
F8	2829 (6)	−1038 (11)	3900 (5)	63
P9	2947 (2)	4147 (4)	3673 (2)	20
C10	3267 (9)	2942 (15)	3180 (6)	30
C11	3656 (9)	5690 (15)	3763 (7)	31
C12	1935 (7)	4787 (14)	3119 (5)	19
C13	1776 (8)	6246 (14)	2976 (6)	25
C14	1021 (9)	6663 (14)	2534 (6)	28
C15	414 (8)	5671 (16)	2243 (6)	28
C16	568 (8)	4218 (17)	2371 (6)	28
C17	1323 (8)	3768 (14)	2802 (6)	23
P18	1733 (2)	3926 (3)	4649 (2)	19
C19	778 (8)	3108 (17)	4129 (6)	31
C20	1545 (10)	5837 (16)	4467 (7)	38
C21	1515 (8)	3878 (14)	5378 (6)	25
C22	891 (8)	2993 (14)	5454 (6)	25
C23	718 (9)	2983 (17)	5990 (6)	33
C24	1164 (10)	3918 (17)	6463 (7)	36
C25	1784 (11)	4788 (20)	6389 (7)	46
C26	1953 (10)	4766 (17)	5849 (7)	36
P27	3370 (2)	1606 (4)	5468 (2)	26
C28	3961 (9)	−24 (17)	5410 (7)	40
C29	4047 (9)	2436 (19)	6176 (7)	38
C30	2528 (8)	756 (13)	5688 (6)	21
C31	2486 (8)	827 (15)	6272 (6)	28
C32	1888 (9)	43 (15)	6427 (7)	28
C33	1334 (9)	−795 (17)	6001 (7)	36
C34	1341 (10)	−879 (17)	5419 (7)	39
C35	1934 (10)	−94 (18)	5259 (7)	39
C36	5571 (11)	4813 (19)	2375 (9)	51
C37	6208 (11)	3932 (19)	2308 (7)	42
C38	6538 (10)	2864 (20)	2721 (8)	45
C39	6270 (10)	2649 (18)	3198 (8)	43
C40	5637 (12)	3476 (21)	3262 (9)	49
C41	5292 (10)	4558 (19)	2850 (10)	48

[a] Isotropic values for those atoms refined anisotropically are calculated by using the formula given by: Hamilton, W. C. *Acta Crystallogr.* **1959**, *12*, 609.

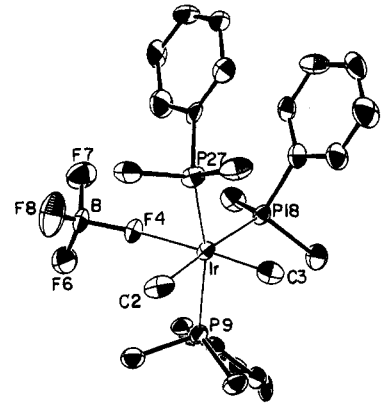

Figure 1. ORTEP drawing of non-hydrogen atoms of $IrMe_2(PMe_2Ph)_3BF_4$, showing atom labeling.

(21) Chatt, J.; Shaw, B. L. *J. Chem. Soc. A* **1966**, 1836.
(22) Shaw, B. L.; Smithies, A. C. *J. Chem. Soc. A* **1967**, 1047.
(23) Lundquist, E. G.; Folting, K.; Huffman, J. C.; Caulton, K. G. *Polyhedron* **1988**, *7*, 2171.
(24) Huffman, J. C.; Lewis, L. N.; Caulton, K. G. *Inorg. Chem.* **1980**, *19*, 2755.

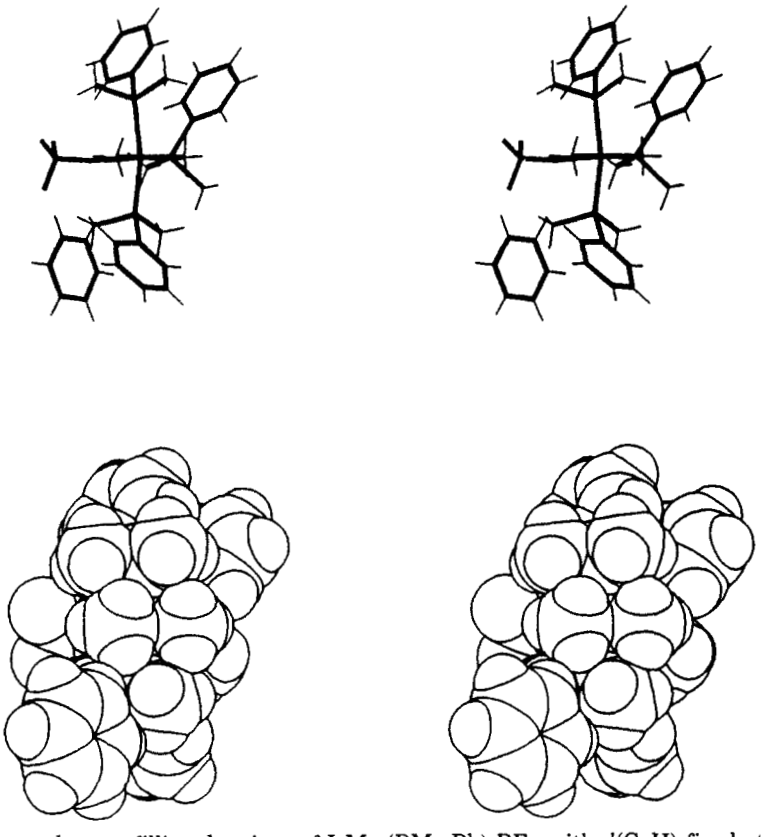

Figure 2. Stereo stick-figure and space-filling drawings of $IrMe_2(PMe_2Ph)_3BF_4$, with d(C–H) fixed at 1.05 Å.

Table III. Selected Bond Distances (Å) and Angles (deg) for $IrMe_2(PMe_2Ph)_3BF_4$

Ir1–P9	2.342 (3)	Ir1–C3	2.083 (14)
Ir1–P18	2.348 (3)	F4–B5	1.436 (17)
Ir1–P27	2.332 (4)	F6–B5	1.352 (19)
Ir1–F4	2.389 (7)	F7–B5	1.382 (19)
Ir1–C2	2.146 (13)	F8–B5	1.356 (19)
P9–Ir1–P18	97.65 (12)	P27–Ir1–C3	92.4 (4)
P9–Ir1–P27	165.06 (12)	F4–Ir1–C2	94.3 (5)
P9–Ir1–F4	84.25 (20)	F4–Ir1–C3	175.8 (4)
P9–Ir1–C2	81.9 (3)	C2–Ir1–C3	87.0 (6)
P9–Ir1–C3	92.1 (4)	Ir1–F4–B5	159.5 (9)
P18–Ir1–P27	96.68 (13)	F4–B5–F6	108.6 (12)
P18–Ir1–F4	89.74 (21)	F4–B5–F7	106.6 (12)
P18–Ir1–C2	175.8 (5)	F4–B5–F8	107.8 (13)
P18–Ir1–C3	88.8 (4)	F6–B5–F7	111.1 (14)
P27–Ir1–F4	91.63 (21)	F6–B5–F8	113.0 (13)
P27–Ir1–C2	84.1 (3)	F7–B5–F8	109.5 (13)

idealized geometries and d(C–H) = 0.95 Å. These calculated positions were fixed for the final cycles of refinement, with the exception of those on the two methyl groups on the Ir. A final difference Fourier was featureless, with several peaks of intensity 1.6 e/Å^3 located near the metal position. Two peaks located near C(3) could be identified as possible hydrogen atoms, but no chemically reasonable peaks were found near C(2). For this reason, no attempt was made to include these methyl hydrogens.

The results of the structural study are shown in Tables II and III and Figures 1 and 2.

***fac*-$RhMe_3(PMe_2Ph)_3$.** To a 40-mL THF solution of *mer*-$RhCl_3P_3$[25] (3.0 g, 4.8 mmol; P = PMe_2Ph) was added 30 mL (45 mmol) of a 1.5 M MeLi/Et_2O solution. The yellow solution initially darkened to red-orange, which gradually faded to a pale yellow. The mixture was slurried for 2 h, cooled to 0 °C, and carefully (dropwise) hydrolyzed with wet THF until gas evolution ceased. After hydrolysis, the solvent was removed under vacuum to give a pale yellow solid. Extraction with CH_2Cl_2 (2 × 25 mL) gave a yellow solution, which was evaporated under vacuum to yield an off-white solid. Washing this material with small amounts of toluene gave 2.0 g (3.6 mmol, 75% yield) of white $RhMe_3P_3$. ^1H NMR (360 MHz, 25 °C, CD_2Cl_2): δ –0.28 (m, 9 H), 1.10 (d, J_{MeP} = 8 Hz, 18 H), 7.0–7.5 (m, Ph–P). $^{31}P\{^1H\}$ NMR (146 MHz, 25 °C, CD_2Cl_2): δ –8.5 (d, J_{PRh} = 80 Hz).

Protonation of *fac*-$RhMe_3P_3$. Generation of $RhMe_2P_3BF_4$. A 5-mm NMR tube was charged with $RhMe_3P_3$ (50 mg, 0.09 mmol) and CD_2Cl_2 (0.5 mL), and against a N_2 flow, 1 equiv of HBF_4·OEt_2 (9 μL, 0.09 mmol) was added. A gas immediately evolved, giving a yellow solution. ^1H NMR spectroscopy indicated quantitative conversion to $RhMe_2P_3BF_4$. ^1H NMR (360 MHz, 25 °C, CD_2Cl_2): δ 0.30 (br s, $Rh(Me)_2$, 6 H), 1.4 (br s, P–Me, 18 H), 7.0–7.5 (m, P–Ph). $^{31}P\{^1H\}$ NMR (146 MHz, 25 °C, CD_2Cl_2): δ 2.5 (br s, 2 P), –16.0 (br s, 1 P). Low-temperature ^1H NMR (360 MHz, –70 °C, CD_2Cl_2): δ 0.25 (br m, Rh–Me, 3 H), 0.35 (br m, Rh–Me, 3 H), 1.4 (br m, P–Me, 12 H), 1.5 (br m, P–Me, 6 H), 7.0–7.5 (m, P–Ph). Low-temperature $^{31}P\{^1H\}$ NMR (146 MHz, –75 °C, CD_2Cl_2): δ 2.5 (d of d, J_{PRh} = 110 Hz, J_{PP} = 17 Hz), –16.0 (d of t, J_{PRh} = 86 Hz, J_{PP} = 17 Hz). ^{19}F NMR (339 MHz, 20 °C, CD_2Cl_2): δ –158 (sharp s). ^{19}F NMR (20 °C, toluene): δ –172 (s). Low-temperature ^{19}F NMR (339 MHz, –80 °C, CD_2Cl_2): δ –158 (sharp s). Low-temperature ^{19}F NMR (–60 °C, toluene): –174 (br s, half-width 680 Hz).

Reaction of $IrMe_2P_3BF_4$ with C_2H_4. A 5-mm medium-walled NMR tube containing 70 mg (0.1 mmol) of $IrMe_2P_3BF_4$ (generated in situ) in CD_2Cl_2 was twice freeze–pump–thaw degassed and then pressurized with 2 atm of C_2H_4 at 25 °C. When the mixture was warmed to 25 °C, it turned yellow and then bleached. ^1H NMR spectroscopy indicated quantitative formation of *cis,mer*-$IrMe_2(C_2H_4)P_3BF_4$. Standing overnight results in formation of large colorless crystals in high yield. In solution, $[IrMe_2(C_2H_4)P_3]BF_4$ loses C_2H_4 in the absence of excess ethylene, regenerating $IrMe_2P_3BF_4$. ^1H NMR (360 MHz, 0 °C, CD_2Cl_2): δ –0.14 (br d of t, $J_{IrMe-P} = J_{IrMe-P'}$ = 7 Hz, 3 H), 0.85 (d of t, $J_{IrMe-P} = J_{IrMe-P'}$ = 8 Hz, 3 H), 1.60 (overlapping m, P–Me, 18 H), 2.85 (s, C_2H_4, 4 H), 7.0–7.6 (m, P–Ph). $^{31}P\{^1H\}$ NMR (146 MHz, –20 °C, CD_2Cl): δ –41.5 (d, J_{PP} = 15 Hz, 2 P), –57.0 (t, J_{PP} = 15 Hz, 1 P). $^{13}C\{^1H\}$ NMR for $[IrMe_2(^{13}C_2H_4)P_3]BF_4$ (146 MHz, 20 °C, CD_2Cl_2): δ 64 (br s, IrC_2H_4).

Crystallography of $[IrMe_2(C_2H_4)(PMe_2Ph)_3]BF_4$. A suitable crystal, grown as described above, was transferred to the

(25) Chatt, J.; Johnson, N. P.; Shaw, B. L. *J. Chem. Soc.* **1964**, 2508.

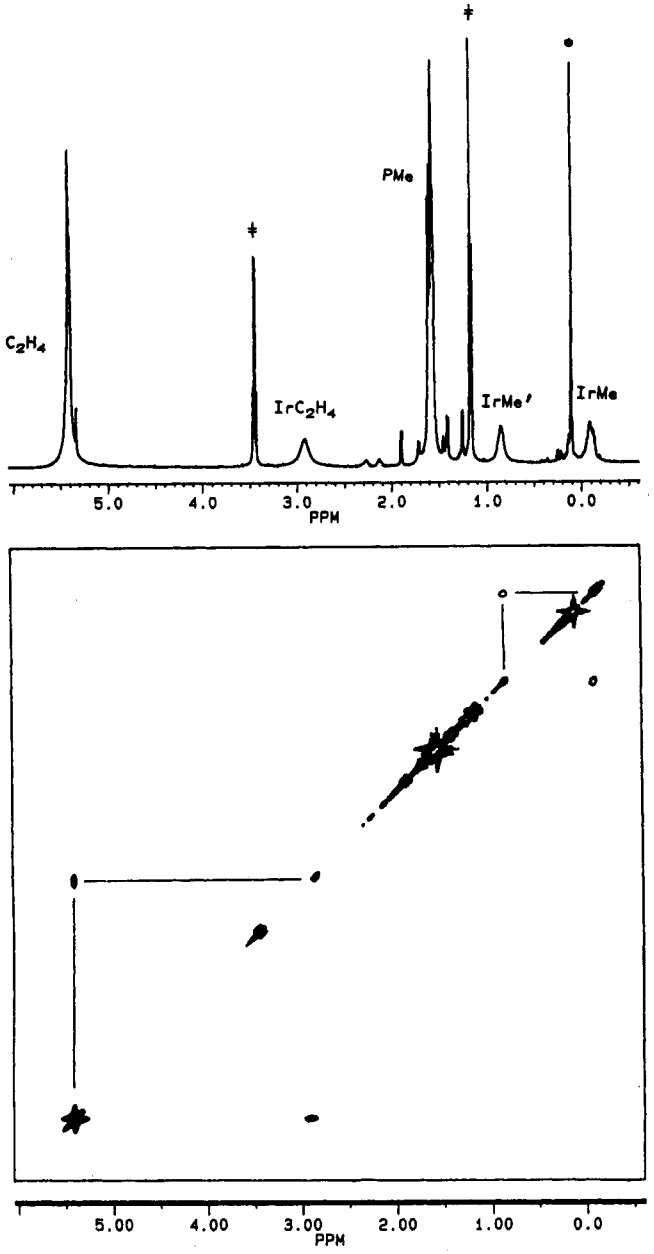

Figure 3. NOESY ^1H NMR spectrum (500 MHz, 25 °C, CD_2Cl_2) of $IrMe_2(C_2H_4)(PMe_2Ph)_3^+$ in the presence of C_2H_4. Cross peaks (off-diagonal) show site exchange of free with coordinated C_2H_4 as well as between the two IrMe sites (‡ indicates Et_2O, and * indicates silicone grease).

goniostat with use of standard inert-atmosphere handling techniques and cooled to −155 °C for characterization (Table I) and data collection.

A systematic search of a limited hemisphere of reciprocal space located a set of diffraction maxima with symmetry and systematic absences corresponding to one of the orthorhombic space groups *Pmcn* and $P2_1cn$. Subsequent solution and refinement of the structure confirmed the noncentrosymmetric choice, $P2_1cn$.

Data were collected ($6° \leq 2\theta \leq 45°$), with use of a continuous θ–2θ scan with fixed backgrounds, and reduced to a unique set of intensities and associated σ values in the usual manner.[24] The structure was solved by a combination of direct methods (MULTAN78) and Fourier techniques. A difference Fourier synthesis revealed the location of some, but not all, hydrogen atoms. All hydrogen atom positions were therefore calculated by using idealized geometries and d(C–H) = 0.95 Å. These calculated positions were fixed for the final cycles of refinement.

An interesting dilemma occurs in that the molecule (including methyl and phenyl groups) possesses nearly perfect mirror symmetry. A careful examination reveals that the chosen space group is undoubtedly correct, but packing diagrams reveal an interesting pseudosymmetry, with the molecules aligned along the diagonals of the proper cell. It is possible that the crystal lies near a phase transition to a different space group. The BF_4^- ions, however, are well-behaved and do not lie on the pseudosymmetry present.

The results of the structure determination are shown in Tables IV and V and Figure 4.

Table IV. Fractional Coordinates and Isotropic Thermal Parameters[a] for $[IrMe_2(C_2H_4)(PMe_2Ph)_3]BF_4$

	10^4x	10^4y	10^4z	$10B_{iso}$, Å^2
Ir1	−8562[b]	−7571 (1)	−9795.4 (4)	11
P2	−8633 (8)	−7422 (4)	−8477 (2)	10 (1)
C3	−8836 (19)	−8658 (21)	−7981 (15)	24 (6)
C4	−7424 (20)	−7013 (21)	−8027 (14)	14 (5)
C5	−9474 (20)	−6480 (22)	−8062 (15)	16 (5)
C6	−9291 (20)	−5426 (21)	−7935 (14)	17 (5)
C7	−9974 (18)	−4658 (18)	−7686 (13)	8 (4)
C8	−10985 (33)	−5017 (26)	−7517 (22)	19 (5)
C9	−11158 (27)	−6106 (27)	−7686 (18)	31 (6)
C10	−10457 (20)	−6817 (21)	−7922 (15)	18 (5)
P11	−9753 (7)	−8998 (6)	−9880 (4)	15 (1)
C12	−10317 (28)	−9189 (27)	−10782 (18)	39 (7)
C13	−9296 (23)	−10371 (23)	−9684 (16)	25 (6)
C14	−10922 (18)	−8943 (18)	−9330 (13)	12 (4)
C15	−11032 (20)	−9608 (20)	−8739 (14)	17 (5)
C16	−11934 (21)	−9515 (19)	−8289 (15)	15 (5)
C17	−12629 (19)	−8696 (19)	−8504 (13)	14 (5)
C18	−12492 (22)	−8052 (21)	−9072 (15)	22 (5)
C19	−11622 (21)	−8175 (20)	−9491 (15)	20 (5)
P20	−7341 (7)	−6191 (6)	−9979 (5)	13 (1)
C21	−6049 (25)	−6528 (24)	−9795 (17)	33 (6)
C22	−7166 (27)	−5678 (25)	−10897 (18)	35 (6)
C23	−7538 (22)	−4880 (21)	−9480 (15)	21 (5)
C24	−8286 (19)	−4193 (18)	−9655 (13)	20 (5)
C25	−8415 (31)	−3204 (19)	−9280 (14)	32 (6)
C26	−7791 (21)	−2947 (21)	−8738 (16)	24 (5)
C27	−6980 (22)	−3595 (22)	−8537 (15)	26 (5)
C28	−6852 (19)	−4572 (19)	−8944 (14)	15 (5)
C29	−9817 (32)	−6338 (30)	−9672 (22)	41 (7)
C30	−9594 (21)	−6502 (22)	−10423 (15)	20 (5)
C31	−8130 (17)	−8082 (18)	−10881 (13)	11 (4)
C32	−7422 (26)	−8733 (23)	−9557 (17)	24 (6)
B33	5447 (29)	3681 (30)	2083 (20)	29 (7)
F34	6234 (13)	3675 (18)	2511 (18)	90
F35	5244 (14)	2701 (14)	1767 (11)	46
F36	4677 (19)	4242 (28)	2275 (17)	107
F37	5704 (37)	4331 (30)	1532 (20)	155

[a] See footnote *a* of Table II. [b] Not varied.

Table V. Selected Bond Distances (Å) and Angles (deg) for $[IrMe_2(C_2H_4)(PMe_2Ph)_3]BF_4$

Ir1–P2	2.400 (5)	Ir1–C32	2.13 (3)
Ir1–P11	2.368 (8)	F34–B33	1.31 (4)
Ir1–P20	2.373 (8)	F35–B33	1.36 (4)
Ir1–C29	2.27 (4)	F36–B33	1.29 (4)
Ir1–C30	2.216 (27)	F37–B33	1.32 (5)
Ir1–C31	2.146 (23)	C29–C30	1.41 (5)
P2–Ir1–P11	95.39 (28)	C29–Ir1–C30	36.6 (11)
P2–Ir1–P20	96.5 (3)	C29–Ir1–C31	118.9 (12)
P2–Ir1–C29	79.8 (10)	C29–Ir1–C32	162.6 (11)
P2–Ir1–C30	116.3 (8)	C30–Ir1–C31	82.4 (10)
P2–Ir1–C31	161.3 (6)	C30–Ir1–C32	160.8 (11)
P2–Ir1–C32	82.9 (9)	C31–Ir1–C32	78.4 (11)
P11–Ir1–P20	168.11 (23)	Ir1–C29–C30	69.7 (19)
P11–Ir1–C29	90.0 (10)	Ir1–C30–C29	73.7 (19)
P11–Ir1–C30	89.1 (7)	F34–B33–F35	114. (3)
P11–Ir1–C31	84.6 (6)	F34–B33–F36	119. (3)
P11–Ir1–C32	90.1 (8)	F34–B33–F37	104. (4)
P20–Ir1–C29	92.8 (10)	F35–B33–F36	115. (3)
P20–Ir1–C30	86.3 (7)	F35–B33–F37	105. (3)
P20–Ir1–C31	83.9 (6)	F36–B33–F37	95. (4)
P20–Ir1–C32	90.6 (9)		

Reaction of $[IrMe_2(^{13}C_2H_4)P_3]BF_4$ with Ethylene. A 5-mm medium-walled NMR tube containing 0.046 mmol of $IrMe_2(^{13}C_2H_4)P_3^+$ (generated in situ) in CD_2Cl_2 under 2 atm of $^{13}C_2H_4$ was heated in a 50 °C oil bath for 12 h. ^1H NMR spectroscopy revealed the formation of $Ir(^{13}C_2H_4)_2P_3]BF_4$[6] and $^{12}C_2H_6$ (0.85

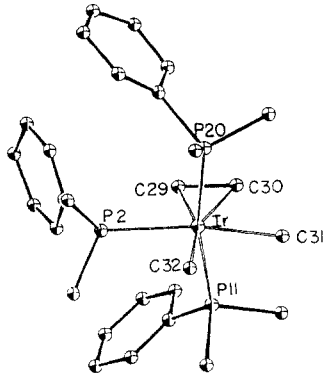

Figure 4. ORTEP drawing of non-hydrogen atoms in $IrMe_2(C_2H_4)(PMe_2Ph)_3^+$, showing atom labeling.

ppm). The $^{13}C\{^1H\}$ NMR spectrum confirmed that no other labeled products were present.

Reaction of $IrMe_2P_3BF_4$ with CO (1 atm): $[IrMe_2(CO)P_3]BF_4$. To a degassed 10-mL CH_2Cl_2 solution of $IrMe_2P_3BF_4$ (150 mg, 0.21 mmol), generated in situ, was added excess CO, but at 1 atm. The yellow solution immediately bleached and was stirred for 2 h. Removal of solvent and excess CO under vacuum afforded a white powder. This powder was washed with THF (only slight solubility) and collected by filtration to yield 150 mg (95% yield) of *cis,mer*-$[IrMe_2(CO)P_3]BF_4$. ^1H NMR (360 MHz, 25 °C, CD_2Cl_2): δ 0.22 (d of t, $J_{IrMe-P} = J_{IrMe-P'} = 9$ Hz, 3 H), 0.26 (d of t, $J_{IrMe-P} = 4.5$ Hz, $J_{IrMe-P} = 9$ Hz, 3 H), 1.35 (d, $J_{MeP} = 9$ Hz, 6 H), 1.60 (vt, $J_{MeP} = 4$ Hz, 6 H), 1.70 (vt, $J_{MeP} = 4$ Hz, 6 H), 7.0–7.65 (m, P–Ph). $^{31}P\{^1H\}$ NMR (146 MHz, 25 °C, CD_2Cl_2): δ −40.4 (d, $J_{PP} = 15.5$ Hz, 2 P), −52.4 (t, $J_{PP} = 15.5$ Hz, 1 P). IR (Nujol mull, ν_{CO}): 2020 cm^{-1}. $^{13}C\{^1H\}$ NMR for $IrMe_2(^{13}CO)P_3^+$ (100 MHz, 25 °C, CD_2Cl_2): δ 172 (d of t, $J_{^{13}CO-P} = J_{^{13}CO-P'} = 7$ Hz).

Reaction of $[IrMe_2(CO)P_3]BF_4$ with Excess CO: $[IrMe(COMe)P_3]BF_4$. A 5-mm medium-walled NMR tube containing 30 mg (0.04 mmol) of the BF_4^- salt of $IrMe_2(CO)P_3^+$ in CD_2Cl_2 was degassed and then pressurized (~3 atm) with excess CO. After 4 h, ^1H NMR spectroscopy of this sealed tube indicates a 20% conversion to $IrMe(COMe)(CO)P_3^+$. No further conversion occurs even after 12 h. ^1H NMR (360 MHz, 20 °C, CD_2Cl_2): δ 0.26 (d of t, $J_{IrMe-P} = J_{IrMe-P'} = 7$ Hz, 3 H), 1.55 (d, $J_{Me-P} = 9$ Hz, 6 H), 1.57 (vt, $J_{MeP} = 4$ Hz, 6 H), 1.78 (vt, $J_{MeP} = 4$ Hz, 6 H), 1.84 (s, COMe, 3 H), 7.0–8.0 (m, P–Ph). $^{31}P\{^1H\}$ NMR (146 MHz, 22 °C, CD_2Cl_2): δ −36.0 (d, $J_{PP} = 16.8$ Hz, 2 P), −50.5 (t, $J_{PP} = 16.8$ Hz, 1 P). IR (Nujol mull): 2015 s, 1600 s cm^{-1}. $^{13}C\{^1H\}$ NMR for $IrMe(^{13}COMe)(^{13}CO)P_3^+$ (100 MHz, 22 °C, CD_2Cl_2): δ 172 (d of t of d, $J_{^{13}CO-^{13}COMe} = 33$ Hz, $J_{^{13}CO-P} = 8.5$ Hz, $J_{^{13}CO-P} = 4$ Hz), 231 (d of m, $J_{^{13}COMe-^{13}CO} = 33$ Hz).

Reaction of $RhMe_2P_3BF_4$ with C_2H_4. A 5-mm medium-walled NMR tube containing 60 mg (0.11 mmol) of $RhMe_2P_3BF_4$ (generated in situ) in CD_2Cl_2 (0.5 mL) was degassed and then pressurized with 2 atm of C_2H_4. After the tube was sealed and the mixture warmed to 25 °C, the yellow solution darkened to yellow-orange. ^1H NMR spectroscopy revealed the presence of ethane (0.85 ppm), ethylene (5.25 ppm), $[Rh(PMe_2Ph)_4]BF_4$,[26] and a small amount of PMe_2Ph.

Reaction of $RhMe_2P_3BF_4$ with CO in THF. A 5-mm NMR tube containing 75 mg (0.14 mmol) of $RhMe_2P_3BF_4$ (generated in situ) in THF (0.6 mL) was degassed and then pressurized with excess CO at −196 °C. The tube was sealed and warmed to 25 °C; the yellow solution pales and then deposits colorless crystals. The tube was kept at −20 °C overnight to afford additional crystals along with a white powder. ^1H NMR spectroscopy confirms that both the crystals and powder are *cis,mer*-$[RhMe_2(CO)P_3]BF_4$. Evacuating a solution of $RhMe_2(CO)P_3^+$ regenerates $RhMe_2P_3BF_4$; in solution under N_2, slow decarbonylation also occurs. ^1H NMR (360 MHz, 20 °C, CD_2Cl_2): δ 0.20 (m, $RhMe_2$, 6 H), 1.20 (d, $J_{MeP} = 9$ Hz, 6 H), 1.40 (vt, $J_{MeP} = 4$ Hz, 6 H), 1.60 (vt, $J_{MeP} = 4$ Hz, 6 H), 7.0–7.5 (m, P–Ph). $^{31}P\{^1H\}$ NMR (146 MHz, 20 °C, CD_2Cl_2): δ −1.0 (d of d, $J_{PRh} = 98$ Hz, $J_{PP} = 23$ Hz, 2 P) −17.0 (d of t, $J_{PRh} = 76$ Hz, $J_{PP} = 23$ Hz, 1 P). IR (Nujol mull): 2055 cm^{-1}. $^{13}C\{^1H\}$ NMR for $[RhMe_2(^{13}CO)P_3]BF_4$ (100 MHz, 20 °C, CD_2Cl_2): δ 188 (d of d of t, $J_{^{13}CO-Rh} = 45$ Hz, $J_{^{13}CO-P} = J_{^{13}CO-P'} = 9$ Hz).

Reaction of $[RhMe_2(CO)P_3]BF_4$ with CO in CH_2Cl_2. A 5-mm medium-walled NMR tube containing 30 mg (0.45 mmol) of $RhMe_2(CO)P_3^+$ in CD_2Cl_2 was degassed and then pressurized with excess CO. After 2 h, the colorless solution had turned yellow-orange and ^1H NMR spectroscopy revealed the presence of only acetone (2.00 ppm) and $[Rh(PMe_2Ph)_4]BF_4$. Identification as acetone was confirmed by rerecording the ^1H NMR spectrum after addition of acetone.

Reaction of $[RhMe_2(CO)P_3]BF_4$ with C_2H_4. A 5-mm medium-walled NMR tube containing 28 mg (0.04 mmol) of $RhMe_2(CO)P_3^+$ was degassed and then pressurized with 2 atm of ethylene. Monitoring (^1H NMR) this reaction over a 24-h period revealed the gradual disappearance of signals for $RhMe_2(CO)P_3^+$ with the appearance of acetone and $[Rh(PMe_2Ph)_4]BF_4$ (also identified by ^{31}P NMR spectroscopy and X-ray diffraction[26]).

Results

Synthesis of $MMe_3(PMe_2Ph)_3$ (M = Ir, Rh). The polyalkyl complex $IrMe_3P_3$ (P = PEt_3, PEt_2Ph) was first prepared by Chatt and Shaw[21] by refluxing a solution of *mer*-$IrCl_3P_3$ with an excess of MeMgCl in benzene. This method produces the facial trimethyl isomer in about 70% yield. It is reported[25,27] that attempts to produce the Rh analogue with this same procedure failed to produce any $RhMe_3L_3$ (L = PR_3). Wilkinson et al.[28] subsequently were successful in preparing $RhMe_3(PMe_3)_3$ in low yield by the reaction of $Rh_2(O_2CCH_3)_4$ with $MgMe_2$ in the presence of excess PMe_3 at low temperatures. In contrast to earlier reports, we did obtain $RhMe_3P_3$ (P ≡ PMe_2Ph) from the reaction of *mer*-$RhCl_3P_3$ with MeMgCl in benzene, although in low (28%) yield. The major product in this reaction is the easily separated complex *cis,mer*-$RhClMe_2P_3$. $RhMe_3P_3$ can, however, be prepared in good yield from the reaction of *mer*-$RhCl_3P_3$[25] with excess MeLi in THF. The facial stereochemistry of this product is easily deduced from the single resonance in the $^{31}P\{^1H\}$ NMR spectrum and the second-order multiplet in the ^1H NMR spectrum due to the magnetic inequivalence of the rhodium methyl groups.

Protonation of MMe_3P_3 (M = Ir, Rh). Generation of $MMe_2P_3BF_4$ and Structure of $IrMe_2P_3BF_4$. Treatment of *fac*-$IrMe_3P_3$ with equimolar $HBF_4 \cdot OEt_2$ in CD_2Cl_2 or C_6D_6 at room temperature gives immediate gas evolution (CH_4 by ^1H NMR). The $^{31}P\{^1H\}$ NMR spectrum of the resulting complex at 20 °C consists of two broad resonances, which sharpen to an AB_2 pattern upon cooling to −80 °C. The ^1H NMR spectrum (CD_2Cl_2) is also temperature-dependent with a single broad IrMe resonance at 0.50 ppm (20 °C) splitting into two separate methyl signals at −80 °C. Similar behavior is observed in both the ^{31}P and ^1H NMR spectra of $RhMe_2P_3BF_4$ produced by stoichiometric protonation of $RhMe_3P_3$ in CD_2Cl_2. Remarkably, both complexes show good solubility in nonpolar solvents such as benzene and toluene.

These observations do not discriminate between a 16e, five-coordinate $IrMe_2P_3^+$ structure and an 18e six-coordinate structure with an agostic methyl group or with coordinated CH_2Cl_2. Moreover, these data and the benzene solubility, in particular, suggest possible coordination of BF_4^-. When pentane is layered into a concentrated benzene solution of $IrMe_2P_3BF_4$, there occurs significant conversion to new materials (by ^{31}P NMR) con-

(26) Lundquist, E. G.; Streib, W. E.; Caulton, K. G. *Inorg. Chim. Acta* **1989**, *159*, 23.

(27) Chatt, J.; Underhill, A. E. *J. Chem. Soc.* **1963**, 2088.

(28) Andersen, R. A.; Jones, R. A.; Wilkinson, G. *J. Chem. Soc., Dalton Trans.* **1978**, 446.

current with deposition of single crystals of $IrMe_2P_3BF_4$. The X-ray diffraction study (Figure 1) reveals this solid to be comprised of the molecular species *cis,mer*-$IrMe_2(PMe_2Ph)_3BF_4$, where the octahedral Ir(III) has inequivalent methyl groups, one of which is trans to η^1-coordinated BF_4.

All Ir–P distances are statistically identical, but the two mutually trans phosphines bend away from P18 toward the methyl of C2. That methyl group has the longer of the two Ir–C bonds (by some 4σ), the shorter Ir–C3 being trans to the weakly bonded η^1-BF_4. There is evidence of graphitic (face-to-face) stacking of the phenyl rings on P18 and P27, and the rotational conformation of the bonds from iridium to P9 and P27 is such as to interleave the attached four *P*-methyl groups with the $IrMe_2$ group (Figure 2).

There is evidence for distortion of BF_4 by coordination. The (μ-F)–B distance is longer than the B–F(terminal) bonds by some 4σ, and the angles (μ-F)–B–F are consistently smaller (106.6 (12)–108.6 (12)°) than the angles between the terminal fluorines (109.5 (13)–113.0 (13)°). The angle at the bridging fluoride is distinctly nonlinear (159.5 (9)°), being bent away from the bulky phosphines and toward C2.

Reactivity of $IrMe_2P_3BF_4$ with C_2H_4. We sought to explore the synthetic utility of $Me_2IrP_3BF_4$ and for this purpose employed the unactivated olefin C_2H_4. The complex in either benzene or CH_2Cl_2 reacts rapidly with C_2H_4 to produce $[IrMe_2(C_2H_4)P_3]BF_4$. The ^1H and ^{31}P NMR spectra in CD_2Cl_2 at 0 and −20 °C, respectively, are consistent with a cis,mer geometry in the cation but, at 25 °C and 500 MHz, the ^1H NMR spectrum shows broad lines for each Ir–Me group and for coordinated and free C_2H_4 (added to prevent conversion to $Me_2IrP_3BF_4$). NOESY two-dimensional ^1H NMR spectra studies show cross peaks (Figure 3) linking free and coordinated ethylene, as well as linking the two inequivalent Ir–Me peaks. These results are consistent with the equilibrium in eq 1, which represents a single (dissociative) mechanism to accomplish both site exchanges, via participation by the 16-electron transient $IrMe_2P_3^+$.

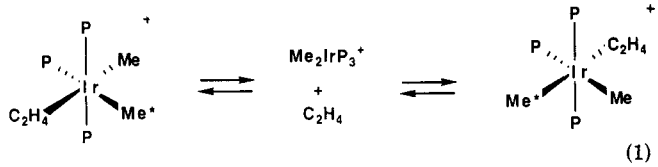

(1)

In an attempt to promote the insertion of ethylene into the cis Ir–Me bond, a CD_2Cl_2 solution containing $IrMe_2(^{13}C_2H_4)P_3^+$ under 2 atm of $^{13}C_2H_4$ was held at 50 °C for 12 h. ^1H NMR spectroscopy indicated the presence of ethane and the formation of the bis(olefin) complex $[Ir(^{13}C_2H_4)_2P_3]BF_4$.[6] $^{13}C\{^1H\}$ NMR spectroscopy confirmed the presence of the bis(olefin) complex and revealed (besides $^{13}C_2H_4$) no other ^{13}C-containing products.

An X-ray diffraction study of $[IrMe_2(C_2H_4)(PMe_2Ph)_3]BF_4$ reveals it to be comprised of noninteracting BF_4^- anions and cis,mer cations (Figure 4). The coordination geometry is approximately octahedral, with some distortions related to the larger (C_2H_4) and smaller (CH_3) ligands. Thus, the cis P–Ir–P angles are 95–97° and the cis H_3C–Ir–CH_3 and H_3C–Ir–P2 angles are 78.4 and 82.9°, respectively. Atoms P11 and P20 likewise bend toward methyl carbon C31, as seen in $IrMe_2P_3BF_4$. The Ir–P2 bond, which is trans to methyl carbon C31, is elongated by 3σ (difference) relative to the other two Ir–P bonds. Similarly, the Ir–C distances to ethylene (2.22 (3) and 2.27 (4) Å) are considerably longer than those (2.14 (2)–2.17 (2) Å) in the closely related Ir(I) complex $Ir(C_2H_4)_2(PMe_2Ph)_3^+$, where there is no methyl group trans to ethylene. Thus, there is structural evidence for a trans bond weakening, which manifests itself in the solution ligand dissociation described by eq 1.

Reactivity of $IrMe_2P_3BF_4$ with CO. $IrMe_2P_3BF_4$ reacts rapidly with carbon monoxide in either benzene or methylene chloride to produce the dialkyl carbonyl complex *cis,mer*-$[IrMe_2(CO)P_3]BF_4$. ^1H and ^{31}P NMR spectroscopy as well as $^{13}C\{^1H\}$ NMR spectroscopy (obtained with $IrMe_2(^{13}CO)P_3^+$), confirm this static octahedral arrangement. The solution infrared spectrum is also consistent with this formulation, showing a single strong absorbance at 2062 cm^{-1}. Unlike $IrMe_2(C_2H_4)P_3^+$, $IrMe_2(CO)P_3^+$ is resistant to ligand (carbonyl) loss even under vacuum.

Placing $IrMe_2(CO)P_3^+$ under additional CO pressure (>2 atm) gives *partial* conversion to the acyl complex *mer*-$[IrMe(COMe)(CO)P_3]BF_4$ (A). The ^1H NMR spectrum

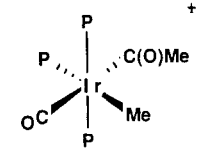

A

shows only one IrMe resonance, as well as a singlet at 1.84 ppm for the acyl methyl. The solid-state infrared spectrum of this equilibrium mixture shows, in addition to absorbances for $IrMe_2(CO)P_3^+$, bands at 2015 and 1600 cm^{-1} for the carbonyl and acyl moieties, respectively. Reacting $IrMe_2P_3BF_4$ with excess ^{13}CO produces $IrMe_2(^{13}CO)P_3^+$ and the doubly labeled cation $IrMe(^{13}COMe)(^{13}CO)P_3^+$. The $^{13}C\{^1H\}$ NMR spectrum reveals a characteristic downfield shift for the acyl group (231 vs 172 ppm for Ir–^{13}CO) with strong (33 Hz) coupling to the trans ^{13}C-labeled carbonyl. In the ^1H NMR spectrum, the acyl methyl is split into a doublet (5 Hz) by the ^{13}C label. The acyl complex spontaneously decarbonylates in the absence of free CO to reform the dimethyl carbonyl complex. Attempts to drive this carbonyl insertion further with use of added ligands other than CO, such as CH_3CN and PMe_2Ph, were unsuccessful.

Reactivity of $RhMe_2P_3BF_4$. Hoping that the insertion of ethylene into a Rh–C bond would be more favorable than with iridium, we investigated the reactivity of $RhMe_2P_3BF_4$ with ethylene. $RhMe_2P_3BF_4$ in CH_2Cl_2 reacts with excess ethylene at room temperature to produce *ethane* and $[Rh(PMe_2Ph)_4]BF_4$. We have previously determined[26] that the RhP_4^+ product in this reaction results from phosphine redistribution of the unsaturated transient species RhP_3^+. Monitoring (by ^1H NMR) the reaction between $RhMe_2P_3BF_4$ and ethylene at low temperature shows no evidence for the formation of the compound $[RhMe_2(C_2H_4)P_3]BF_4$.

In THF, $RhMe_2P_3BF_4$ reacts with carbon monoxide to deposit colorless crystals of *cis,mer*-$[RhMe_2(CO)P_3]BF_4$. This complex possesses spectral properties similar to those of the iridium analogue. Unlike the iridium compound, $RhMe_2(CO)P_3^+$ in solution, under vacuum, loses CO to regenerate $RhMe_2P_3BF_4$. Tetrahydrofuran is thus an especially favorable solvent for preparing $[RhMe_2(CO)P_3]BF_4$, since the compound precipitates spontaneously from this solvent. $RhMe_2(CO)P_3^+$ dissolved in CH_2Cl_2 reacts with added CO to form acetone and a Rh-containing product (eq 2). The rhodium-containing final product is, as found in the reaction of ethylene with $RhMe_2P_3BF_4$, the

$$cis,mer\text{-}RhMe_2(CO)P_3^+ \xrightarrow{L = CO,\ C_2H_4} (CH_3)_2CO + RhP_4^+ + \ldots \quad (2)$$

redistribution product of the RhP_3^+ species: RhP_4^+.[26] Nucleophiles other than CO will also promote the formation of acetone and RhP_4^+. When $RhMe_2(CO)P_3^+$ in CD_2Cl_2 is exposed to an ethylene atmosphere, slow ($t_{1/2}$ = 12 h) reductive elimination of acetone and the formation of RhP_4^+ are observed.

Discussion

The overwhelming majority of apparent 16-electron complexes of the "middle" transition elements contain potential π-donor ligands (halogen, OR, SR, NO, etc.). It is thus quite exceptional to find isolable unsaturated complexes containing only phosphine and alkyl or hydride ligands. The 16-valence-electron complexes $MMe_2P_3^+$ (M = Rh, Ir), produced by protonation of MMe_3P_3 with HBF_4, are in accord with this general situation. In the solid state, BF_4 is η^1-coordinated, forming *cis,mer*-$IrMe_2(FBF_3)P_3$ and affording the Ir(III) d^6 center a preferred octahedral environment. The distortion of BF_4 upon coordination is similar to that found in $Cu(PPh_3)_3FBF_3$ and *trans*-$IrH(PPh_3)_2Cl(CO)(FBF_3)$ with an elongation of the (μ-F)–B distance over that of the B–F(terminal) bonds. The B–F–Ir angle of 159.5° is, however, markedly more linear than the M–F–B angle found for *trans*-$IrH(PPh_3)_2Cl(CO)(FBF_3)$ (125.7°),[16] probably as a result of steric repulsions between FBF_3 and the *three* phosphine ligands. The Ir–F distance of 2.39 Å is over 0.1 Å longer than in $IrH(PPh_3)_2Cl(CO)(FBF_3)$, showing the weakness of this interaction.

In CH_2Cl_2 solvent, the ^{19}F NMR spectrum of $IrMe_2P_3BF_4$ shows a single line at the chemical shift of free BF_4^-. This chemical shift is unchanged down to −90 °C. These observations suggest essentially complete separation of cation and anion in CH_2Cl_2; we cannot state whether the cation is 18-electron $IrMe_2(CH_2Cl_2)P_3^+$ or 16-electron $IrMe_2P_3^+$. One additional subtle feature demands interpretation: the $^{31}P\{^1H\}$ resonance of $IrMe_2P_3BF_4$ in CH_2Cl_2 shows well defined P/P coupling at −90 °C, but this is unresolved (due to broad lines) at 19 °C. Similarly, the Me–P ^1H NMR signals are broad at 25 °C. We interpret this as indicating the coexistence of two distinct species at 19 °C; these interconvert at an intermediate exchange rate. One of these could be a small fraction of the η^1-BF_4 species seen in the solid state.

In contrast, in benzene or toluene solvent, there is spectral evidence (in addition to solubility behavior) for retention of η^1-BF_4. First, the ^{31}P chemical shifts of $IrMe_2P_3BF_4$ in toluene are 6–10 ppm downfield of their values in CH_2Cl_2. When the temperature in toluene is lowered, a broadening of the ^{19}F signal is observed for $IrMe_2P_3BF_4$. At −90 °C, the resonance has shifted upfield by 15 ppm to −185 ppm and has a width at half-height of 6800 Hz. For comparison, Beck has obtained low-temperature ^{19}F NMR data (CD_2Cl_2) in which separate resonances for the bridging and terminal fluorides are observed.[15] For instance, the complex $Cp(CO)_3MoFBF_3$ at −80 °C shows a doublet at −156 ppm for the terminal fluorides and a quartet at −372 ppm for the bridging fluoride. However, in $CpFe(CO)_2(\eta^1\text{-}BF_4)$, bridging and terminal F differ by only 13 ppm.[13] While separate ^{19}F signals for $IrMe_2P_3FBF_3$ in toluene are not frozen out at −90 °C, a definite BF_4 interaction is inferred from the extremely broad nature of the ^{19}F resonance. Although this broadening is consistent with a terminal-to-bridging fluoride-exchange process that has a low energy barrier, the fact that this average chemical shift is *altered* upon cooling necessitates the simultaneous occurrence of an equilibrium process. An equilibrium between a coordinated BF_4 and a solvent-separated BF_4 would account for this observation.

The proposed coordination of a ligand as poor as CH_2Cl_2 demonstrates the high Lewis acidity of a 16-electron complex devoid of π-donor ligands. Nevertheless, authentic 16-electron $IrMe_2P_3^+$ is of central importance as a transient in the fluxionality (eq 1) (unusual for a d^6 octahedron) and reactivity of $IrMe_2P_3BF_4$.

The coordinated BF_4^- is easily replaced by ethylene, forming *cis,mer*-$[IrMe_2(C_2H_4)P_3]BF_4$. A NOESY two-dimensional NMR experiment on this complex reveals methyl site exchange by an ethylene dissociation process and again implicates the fluxional $IrMe_2P_3^+$ species. The fluxional behavior of $[IrMe_2(C_2H_4)P_3]BF_4$ is again rare for a d^6 octahedral compound and is in contrast to that for the recently reported isoelectronic, stereochemically rigid complex *cis,mer*-$[IrH_2(C_2H_4)(PMe_2Ph)_3]BF_4$. The Beck group has similarly reported the displacement of coordinated BF_4 by ethylene with the formation of the thermally unstable complex *trans*-$HIr(PPh_3)_2(CO)(C_2H_4)Cl^+$. The solid-state X-ray structure determination of $IrMe_2(C_2H_4)P_3^+$ reveals an octahedral structure with ethylene coplanar with the two methyl groups and the unique phosphine phosphorus. The BF_4 is well separated and tetrahedral. The C=C(ethylene) distance of 1.41 Å compares with other transition-metal–ethylene complexes; no exceptionally short C–C distance is present, as might be expected for such a weakly held ethylene ligand. Overall, the structure resembles that of $IrMe_2(FBF_3)P_3$ with an ethylene in place of η^1-BF_4. The trans phosphine ligands deviate from a linear arrangement (168°) in an effort to minimize steric interactions with the remaining phosphine ligand. As with $IrMe_2(FBF_3)P_3$, the Ir–C bond for the methyl trans to the weakly coordinated ligand (η^1-BF_4 and C_2H_4) shows a markedly shortened length as compared to that for the other methyl trans to phosphine.

Given the cis ethylene/methyl relationship in $[IrMe_2(C_2H_4)P_3]BF_4$, the possibility of ethylene insertion was anticipated. Heating $IrMe_2(^{13}C_2H_4)P_3^+$ under a $^{13}C_2H_4$ atmosphere overnight results in the formation of $[Ir(^{13}C_2H_4)_2P_3]BF_4$ and ethane without the appearance of any possible ethylene insertion products (e.g. $CH_3{}^{13}CH_2{}^{13}CH_2CH_3$, $^{13}CH_2{=}{}^{13}CHCH_3$.

Carbon monoxide will also displace η^1-BF_4, forming *cis,mer*-$[IrMe_2(CO)P_3]BF_4$. This complex, unlike $IrMe_2(FBF_3)P_3$ and $[IrMe_2(C_2H_4)P_3]BF_4$, is stereochemically rigid and shows no tendency for ligand (CO) dissociation. In the presence of excess CO, $IrMe_2(CO)P_3^+$ is *partially* converted to the acyl complex *mer*-$[IrMe(COMe)(CO)P_3]BF_4$. Even under 2 atm of CO, insertion to produce the acyl complex only proceeds to ca. 20% completion. Deinsertion of CO occurs in solution under vacuum or on standing under N_2 for a period of 2 days and regenerates the dimethyl cation.

The stereochemistry of the acyl complex A, particularly the trans arrangement of the acyl and entering CO ligands, suggests that the C*O that adds to $IrMe_2(CO)P_3^+$ enters between P′ and Me′ (Scheme I), either in the 18-electron carbonyl complex (path a) or in an acyl precursor (path b). That this is the correct stereochemistry of nucleophilic attack is also supported by the fact that, for rhodium, C*O above can be replaced by ethylene and still result in acetone formation.

Although factors that control acyl–alkyl equilibria in iridium(III) complexes are not well understood, Bennett[29]

Scheme I

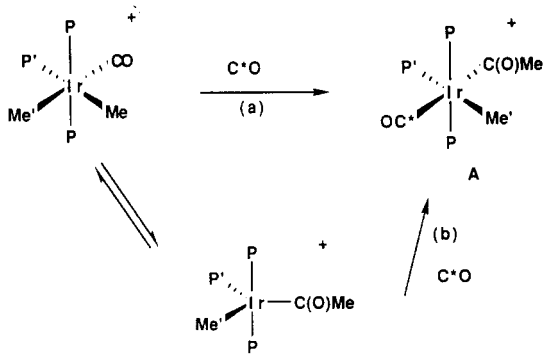

has found that the equilibrium between the five-coordinate acyl complex $Ir(Cl)(COR)(PMe_2Ph)_3^+$ and the six-coordinate alkyl complex *mer*-$Ir(Cl)(R)(CO)(PMe_3Ph)_3^+$ is entirely on the side of the alkyl complex. Our work shows that replacement of chloride with methyl in this complex shifts the equilibrium toward the acyl.

In THF, $RhMe_2P_3BF_4$ reacts with CO to rapidly deposit the THF-insoluble complex *cis,mer*-$[RhMe_2(CO)P_3]BF_4$. When additional CO is added to CH_2Cl_2 solutions of this dimethyl carbonyl cation, the elimination of acetone occurs with the formation of $Rh(PMe_2Ph)_4^+$. Although not observed, it is quite reasonable that a cis methyl acyl complex, similar to that observed for Ir, is the intermediate which proceeds to eliminate acetone under mild conditions.[30] The formation of acetone and not ethane establishes that CO insertion, followed by nucleophile-promoted reductive elimination of acetone, is a faster, more favorable process than simple reductive elimination of ethane. Such behavior finds precedent in the reactivity of $RuR_2(CO)_2P_2$.[31]

The project described here was initiated to produce unsaturated metal complexes containing ligands anticipated to be reactive toward unsaturated nucleophiles (e.g., CO and C_2H_4). The results reported here reveal rather dramatically the differences in the reactivity and stability of analogous rhodium and iridium complexes. As is generally observed, the reactions of the 5d metal are slower than those of a 4d analogue (e.g., eq 3, where $T \leq 25$ °C

$$MMe_2P_3BF_4 + C_2H_4 \xrightarrow{T} C_2H_6 + \ldots \quad (3)$$

for rhodium but $T \geq 50$ °C for iridium). The products are also different. For iridium, the 18-electron trigonal-bipyramidal $Ir(C_2H_4)_2P_3^+$ is obtained. In contrast, the functional unit $Rh(PMe_2Ph)_3^+$ apparently fails to bind ethylene well, and this 14-electron species undergoes a complex phosphine ligand redistribution to generate $Rh(PMe_2Ph)_4^+$. It is remarkable that ethylene is capable of *inducing* reductive elimination of ethane from $RhMe_2P_3BF_4$ but unable to *bind* to RhP_3^+.

When the nucleophile is CO, the reactivity is equally distinct for the two metals. For iridium, carbonylation proceeds through a CO adduct to give a carbonyl–methyl–acetyl species that does not reductively eliminate. For rhodium, the reaction proceeds without *detectable* intermediates to eliminate acetone. However, the excess CO (like C_2H_4) is incapable of stabilizing RhP_3^+, and the same redistribution observed above takes place, to again yield RhP_4^+. $Rh(PMe_2Ph)_3Cl$, upon treatment with $LiBF_4$ in CH_2Cl_2, also produces major amounts of $[Rh(PMe_2Ph)_4]BF_4$. We will report elsewhere on our attempts to inhibit phosphine redistribution using a tridentate phosphine.

All of the above reactions may be classified as nucleophile-induced reductive eliminations. Such reductive eliminations, being the product-releasing step, are integral to several catalytic reactions. In the case of ethylene hydrogenation, we earlier reported[6] that elimination of ethane from $HIrEtP_3^+$ is ethylene-promoted. Here, we observe nucleophile-promoted carbon-carbon reductive eliminations. In the case of CO and rhodium, the nucleophile becomes part of the eliminated molecule but is unable to stabilize the Rh product. The concept of nucleophile promotion of reductive elimination is even effective when that nucleophile does not bind to the products (eq 4) and

$$RhMe_2(CO)P_3^+ \xrightarrow{C_2H_4} Me_2CO + RhP_4^+ + \ldots \quad (4)$$

is thus clearly a kinetic phenomenon. These reductive eliminations are found to be more kinetically facile for rhodium than for iridium, with the corollary benefit that intermediates are readily detected for the sluggish iridium analogues. The availability of unsaturated polyalkyl complexes (or their operational equivalent) by the acidolysis methodology employed here is thus useful in the generation, characterization, and study of reactive organometallic intermediates.

Acknowledgment. This work was supported by a grant from the National Science Foundation. We thank Johnson-Matthey Co. for material support and Scott Horn for skilled technical assistance.

Registry No. *fac*-$IrMe_3P_3$, 15927-48-7; $IrMe_2P_3BF_4$, 127973-72-2; $IrMe_2P_3BF_4 \cdot C_6H_6$, 127973-73-3; *mer*-$RhCl_3P_3$, 14882-42-9; *fac*-$RhMe_3P_3$, 128051-02-5; $RhMe_2P_3BF_4$, 123143-41-9; C_2H_4, 74-85-1; *cis,mer*-$IrMe_2(C_2H_4)P_3BF_4$, 127973-75-5; CO, 630-08-0; *cis,mer*-$[IrMe_2(CO)P_3]BF_4$, 127973-77-7; $[IrMe(COMe)P_3]BF_4$, 127973-79-9; *cis,mer*-$[RhMe_2(CO)P_3]BF_4$, 127973-81-3.

Supplementary Material Available: Listings of anisotropic thermal parameters for $IrMe_2(PMe_2Ph)_3BF_4 \cdot C_6H_6$ and $[IrMe_2(C_2H_4)(PMe_2Ph)_3]BF_4$ (2 pages); listings of observed and calculated structure factors (16 pages). Ordering information is given on any current masthead page.

(29) Bennett, M. A.; Jeffrey, J. C.; Robertson, G. B. *Inorg. Chem.* **1981**, *20*, 323.
(30) The *intra*molecularity of the elimination process has not been proven here.
(31) Saunders, D. R.; Mawby, R. J. *J. Chem. Soc., Dalton Trans.* **1984**, 2133.